

1 Atmospheric Mixed Rossby Gravity Waves over Tropical Pacific

2 during the Austral Summer

3 Hugo A. Braga¹ and Victor Magaña¹

4 ¹Departamento de Geografía Física, Instituto de Geografía, Universidad Nacional Autónoma de México, 04510, México
5 City, México.

6 *Correspondence to:* Hugo A. Braga (hugoalvesbraga@icloud.com)

7 **Abstract.** Atmospheric Mixed Rossby-Gravity Wave (MRGW) activity during the austral summer months (Dec-Jan-Feb) is
8 examined by means of observational analyses for the 1991 - 2020 period. The main objective of the study is to explore the
9 relationship between tropical circulations at upper and lower tropospheric levels and tropical convective activity. Using an
10 Empirical Orthogonal Function (EOF) analysis of the high-frequency meridional component anomalies of the wind at 200
11 hPa, for zonal wavenumber 4-6, episodes of intense MRGW activity are detected. Composite analyses based on an EOF
12 analysis show a quadrature phase over the central-eastern equatorial Pacific between the MRGW structure in the upper and
13 lower troposphere. Lagged correlations between the first two EOFs principal components, and the wind field and OLR, show
14 that MRGWs are laterally forced at upper tropospheric levels over the westerly duct region and later propagate westward and
15 downward. Once the MRGW reaches the lower tropospheric levels, it induces zones of moisture convergence that modulate
16 convective activity. Tropical convection develops in the MRGW moisture convergence region at 700 hPa and the divergent
17 region of the wave at 200 hPa. Since the MRGW phase tilts eastward with height, moisture convergence at lower
18 tropospheric levels tends to coincide with divergence at upper levels favouring intense convective activity which results in
19 the antisymmetric outgoing longwave radiation anomalies observed off the equator near the MRGW. Therefore, the
20 occurrence of MRGWs over the eastern Pacific, is a form of tropical – extratropical interaction that generates tropical
21 convection anomalies by means of induced lower tropospheric moisture convergence and divergence anomalies.

22 **Keywords:** Mixed Rossby-Gravity Waves, Tropical–Extratropical Interactions, Lateral Forcing, Moisture Convergence.

23 1 Introduction

24 Equatorial waves are important elements of the atmospheric tropical circulations. Matsuno (1966) determined the main
25 spatial and temporal characteristics of Mixed Rossby-Gravity Waves (MRGWs), later identified by means of observational
26 analyses by Yanai and Maruyama (1966) and Maruyama (1967). In the present study, MRGWs will refer to the westward
27 moving waves in the troposphere, coupled with tropical convection, as those discussed by Magaña and Yanai (1995). Various
28 observational studies show that MRGWs exhibit fluctuations in the meridional component of the wind, with periods between

29 4 to 6 days and zonal wave numbers 4 to 6 (Yanai and Hayashi 1969; Yanai and Murakami 1970a, b; Nitta 1970). Their
30 vertical wavelengths range between 6 to 10 km (Holton 1979, Magaña and Yanai 1995) with an upward propagation from the
31 upper troposphere to lower stratospheric levels (Yanai and Hayashi, 1969).

32 The origin of MRGWs indicates that lateral forcing is a common trigger of MRGWs, as originally proposed in model studies
33 by Mak (1969) and later explored by Bennet and Young (1971), Hayashi and Golder (1978) and Zhang and Webster (1992),
34 among others. Observationally, Yanai and Lu (1983), Magaña and Yanai (1995), Yang and Hoskins (2016), Kiladis et al.
35 (2016), Yang et al. (2018), Suhas et al. (2020) and Shreya and Suhas (2024) also documented MRGWs triggered by lateral
36 forcing. On the other hand, tropical convective heating has also been suggested as a mechanism that results in MRGWs
37 (Holton, 1972; Hess et al., 1993). Hayashi (1970) proposed that MRGWs could be the result of Wave-CISK, i.e., by means
38 of the interaction between convective heating and the wave itself. However, Takayabu and Nitta (1993) ruled out
39 Wave-CISK as a mechanism to maintain MRGWs. In any event, the relationship between MRGWs and tropical convective
40 activity exists (e.g., Magaña and Yanai 1995, Kiladis et al., 2009), but a definite answer how it works has not been given.

41 The first observational studies on the vertical structure of MRGWs indicate that they extend from the troposphere to the
42 lower stratosphere (Yanai and Hayashi, 1969). A vertical node of these equatorial waves appears in the upper-tropospheric
43 level (around 200 hPa), and the phase tilts westward to lower tropospheric levels and eastward into the stratosphere (Magaña
44 and Yanai 1995; Zhou and Wang 2007; Kiladis et al., 2009). The tilting of MRGWs plays a crucial role in the vertical
45 transport of momentum and energy (Holton, 1979), but it may also be important in the spatial distribution of the convective
46 activity anomalies associated with MRGWs (Kiladis et al., 2009).

47 The triggering of MRGWs by midlatitude disturbances from the winter hemisphere takes place in the eastern Pacific
48 westerly duct (Webster and Holton, 1982), which tends to remain “open” in the upper troposphere during the austral summer
49 months (Dec-Jan-Feb) (Braga et al., 2022). During the boreal summer (Jun-Jul-Aug) the westerly duct forms periodically as
50 the Madden Julian Oscillation propagates along the eastern tropical Pacific, which allows the formation of MRGWs (Magaña
51 and Yanai, 1991). Therefore, it is expected that MRGWs triggered by later forcing be more frequent during the austral
52 summer. Their signal at lower atmospheric levels though may be more evident in the region of westerlies, close to the
53 western Pacific (Au-Yeung and Tam, 2018). Consequently, we will focus on this temporal period to examine the relationship
54 between MRGWs triggered in the upper troposphere that extend the signal to lower tropospheric levels in relation to the
55 development of tropical convection.

56 A study by Zhou and Wang (2007) shows that an upper tropospheric MRGW acts as the precursor to a western Pacific
57 tropical depression. Consequently, the downward phase propagation and the vertical structure of the MRGW should be
58 considered in the development of a region of intense convective activity around the equatorial wave. These analyses suggest
59 that an upper tropospheric MRGW may reflect in the modulation of moisture convergence and divergence near the boundary
60 layer, that ultimately controls deep convective activity in the equatorial regions. Consequently, the existence of MRGWs and
61 the corresponding antisymmetric anomalies in convective activity (Kiladis et al., 2009) may be considered part of the
62 evolution of MRGW from upper to lower tropospheric levels.

63 The present study aims at examining the characteristics and evolution of MRGWs, in the Pacific region, and the relationship
64 between this type of equatorial wave and convective activity off the equator, which remains as an open scientific question.
65 This study is structured as follows: Section 2 outlines the characteristics of the data used for the study and the methodology
66 of investigation. In Section 3, observational analyses are developed to determine the characteristics and evolution of
67 MRGWs and their relationship with convective activity. In Section 4 summary and conclusions are presented.

68 **2 Data**

69 **2.1 Data sets**

70 For the identification of MRGWs, global reanalyses of daily tropospheric winds and specific humidity ERA-5 for the period
71 1991 to 2020 (Hersbach et al., 2020) have been used. The spatial resolution of ERA-5 wind data is $2.5^\circ \times 2.5^\circ$ from 1000 to
72 100 hPa. Daily Outgoing Longwave Radiation (OLR) data from the National Oceanic and Atmospheric Administration
73 (NOAA) for the same period were also used (Liebmann and Smith, 1996) to document tropical convective activity
74 anomalies.

75 **2.2 Vertically Integrated Moisture Flux**

76 The vertically integrated moisture flux field and its divergence were calculated to evaluate how atmospheric moisture is
77 distributed by tropical disturbances in the tropical regions. The VIMF is a measure of the amount of water vapor transported
78 in the atmosphere. Its convergence is used in the evaluation of the hydrological processes in the atmosphere (Fasullo and
79 Webster, 2003). High VIMF convergence (VIMFc) zones are related to intense convective activity. The VIMF has been used
80 to examine moisture transport processes, for instance in Easterly Waves (Pazos et al., 2023). The VIMF is calculated using
81 the expression:

$$82 \quad \text{VIMF} = \frac{1}{g} \int_{p=1000}^{p=100} Vqdp \quad (1)$$

83 where q is the specific humidity ($\text{kg}\cdot\text{kg}^{-1}$), V is the horizontal wind field, g is the gravity constant, and p is the pressure
84 between 1000 and 100 hPa. VIMF units are $\text{kg m}^{-1} \text{s}^{-1}$.

85 **2.3 Methodology**

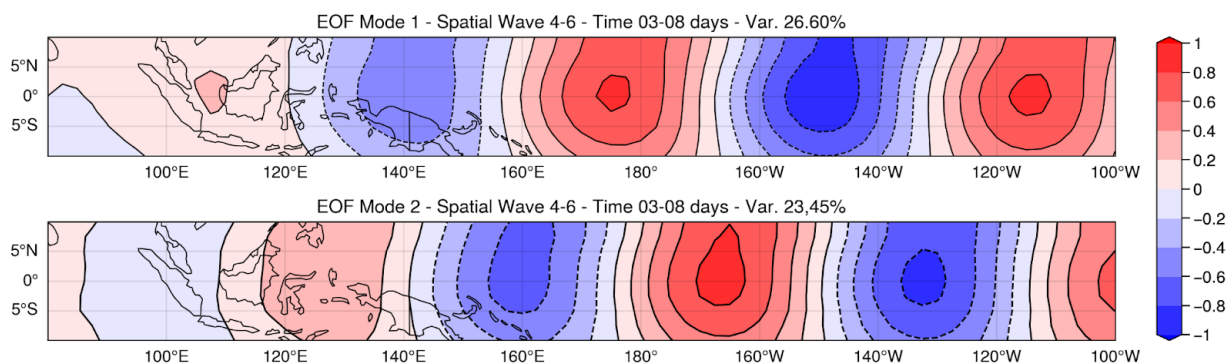
86 Various approaches have been used to diagnose MRGWs activity including spectral analysis with radiosonde data (Yanai and
87 Hayashi, 1969), or reanalysis data (Yanai and Lu, 1983; Magaña and Yanai, 1995; Wheeler and Kiladis, 1999), or by
88 projecting meteorological wind fields of reanalysis data onto the theoretical spatial structures of equatorial waves (Yang et
89 al., 2003; Au-Yeung and Tam, 2018, Knippertz et al., 2022). In this study, MRGWs patterns have been identified by means
90 of Empirical Orthogonal Function (EOF) analyses (Kiladis et al., 2016) of the meridional component of the 200 hPa wind

91 field, based on the covariance matrix. The Principal Components (PC1, PC2) of EOFs are used as indices to compose wind,
 92 OLR, and atmospheric moisture fields to obtain the spatial characteristics of the MRGWs. PC1 and PC2 do not include
 93 variations with periods larger than 90 days, that may appear as interannual variations, result of the use of data for the
 94 Dec-Jan-Feb period. The identification of periods and regions of MRGW activity are determined based on periods of large
 95 signals of PC1 or PC2. The temporal evolution of MRGW is examined by means of lagged – correlations between PC1 or
 96 PC2 and the wind, OLR and moisture fields. Data are band-pass filtered with a Lanczos Filter (Duchon, 1979), in the period
 97 range between 3 and 8 days. The spatial structure of the MRGW in the EOF analysis is captured with a spatial filter for zonal
 98 wavenumbers 4 to 6 (Hayashi, 1982). The wavelength spectrum for the EOF's is limited to the spatial scales, characteristic
 99 of MRGW. The inclusion of larger or smaller zonal wavenumbers may capture other modes present in the tropics. However,
 100 the main focus of this is on a prototype MRGW with zonal wavenumber 4-6.

101 3. Results and Discussions

102 3.1 MRGW Detection

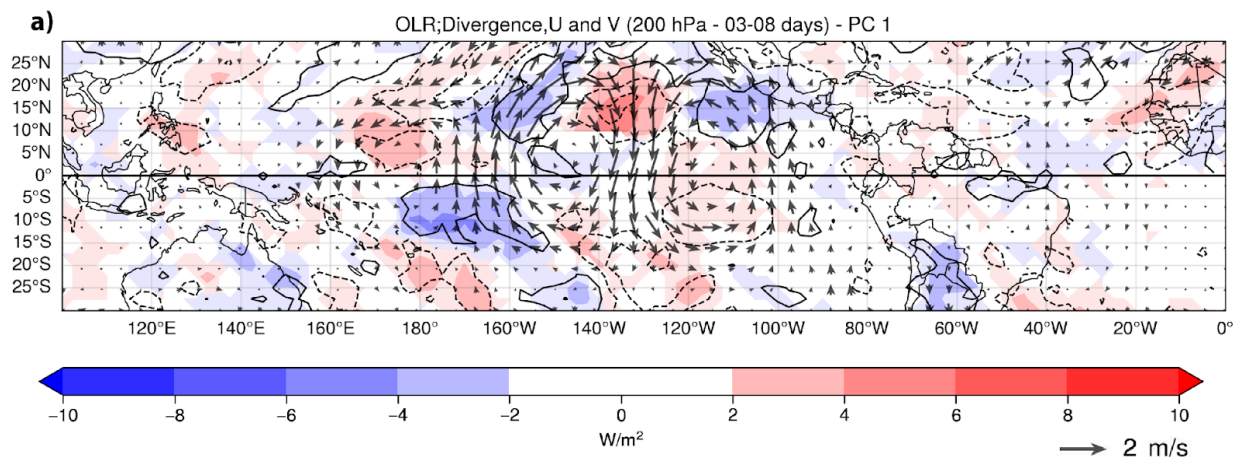
103 The first EOF of the band-pass filtered component of the meridional wind (v) at 200 hPa, spatially filtered in the 4 and 6
 104 zonal wavenumber range, in the 10°N-10°S, 80°E-100°W domain, similar as the one used by Kiladis et al. (2016) and Suhas
 105 et al. (2020), shows the signal of a MRGW with a dominant zonal wavenumber 5 (Fig.1). EOF2 also captures the MRGW
 106 signal, but it is in quadrature with EOF1 (PC2 leads PC1 by approximately 100 degrees) which corresponds to the westward
 107 propagation of the wave. The coherence squared between PC1 and PC2 in the 5 to 8 days period range is around 0.66.

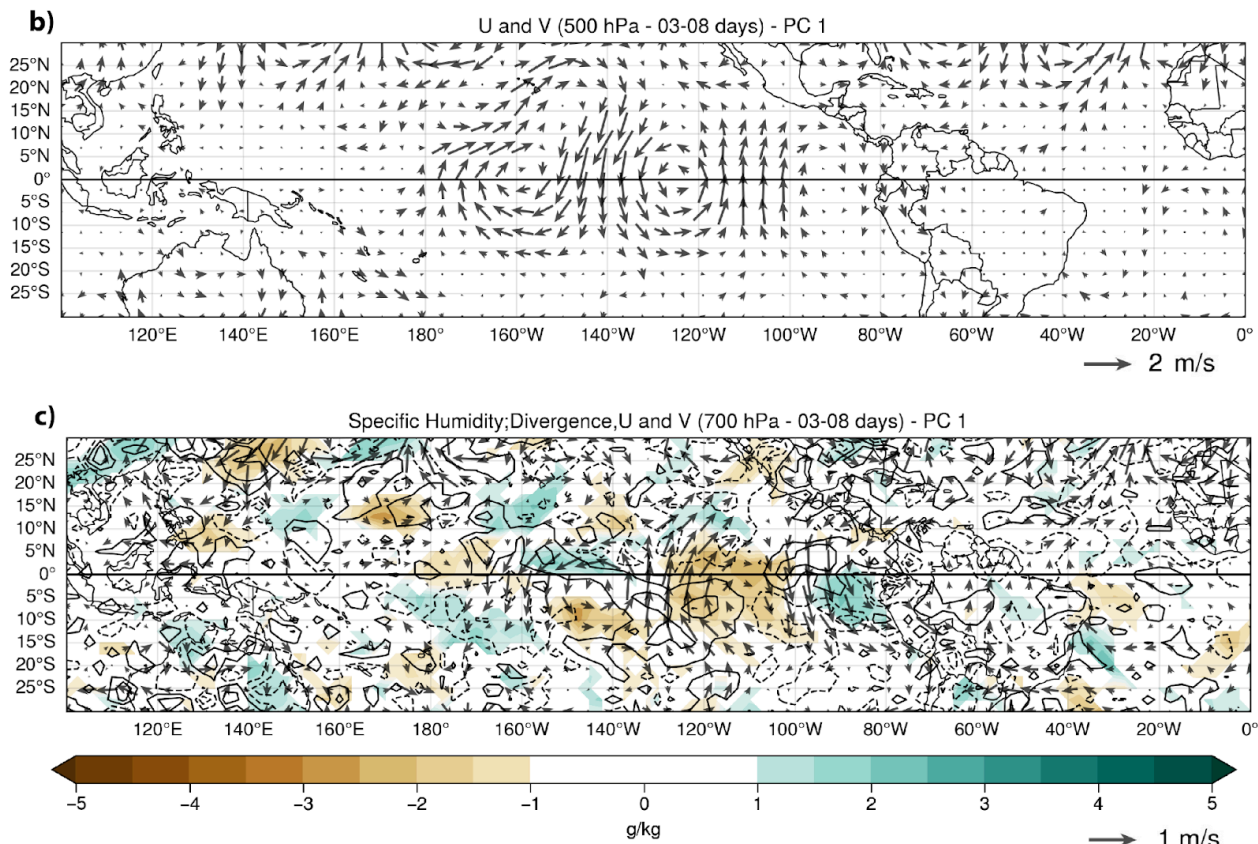


108
 109 **Figure 1: First and second EOF for the 200 hPa space-time filtered anomaly of the meridional component of the wind field at 200**
 110 **hPa for the December to February for the 1991 to 2020 period.**

111 To obtain the spatial structure of the wind field corresponding to a MRGW, composite patterns of the space-time band-pass
 112 filtered wind fields at 200, 500 and 700 hPa were constructed using PC1 values larger than 1.0. The composite of the wind
 113 field was combined with OLR anomalies at upper-levels and specific humidity anomalies at lower levels to obtain the
 114 regions of the induced tropical convective activity (Fig.2). Over the central eastern Pacific, clockwise and anticlockwise
 115 circulations, centred along the equator, show the anomalous wind field of a MRGW (Fig.2.a). In agreement with the

116 theoretical model, its convergent and divergent regions are anti-symmetrically located off the equator in between the
 117 clockwise and anticlockwise circulations. The positive and negative OLR anomalies associated with the MRGW coincide
 118 with the regions of convergence and divergence at upper tropospheric levels. At 500 hPa, the phase of the MRGW over the
 119 central Pacific is displaced around 10° to the west with respect to its 200 hPa counterpart (Fig.2.b), reflecting its eastward tilt
 120 with height in the troposphere (Suhas et. al., 2020). When the signal of the MRGW is calculated at lower tropospheric levels
 121 it is observed there is a further phase shift towards the west in the clockwise and anticlockwise circulations. At 700 hPa, the
 122 intensity of the circulations is weaker than at upper tropospheric levels, but regions of atmospheric moisture convergence
 123 and divergence are observed off the equator in between the cyclonic and anticyclonic circulations. Just above the tropical
 124 boundary layer, the zone of moisture convergence (divergence) is located at 160°W and 5°S to 10°S (5°N to 10°N) and at
 125 around 115°W and 5°N to 10°N (5°S to 10°S), on the west and east sides of the clockwise circulation in the central Pacific
 126 (Fig.2.c). Moisture convergence-divergence leads to increases-decreases of atmospheric humidity that tend to coincide with
 127 the regions of negative-positive OLR anomalies. Such connections between upper and lower tropospheric levels around the
 128 MRGW circulation suggest that tropical convection anomalies are generated at lower tropospheric levels through moisture
 129 convergence, that coincide with regions of divergence and convergence at upper tropospheric levels due to the quadrature in
 130 the MRGW between these two tropospheric levels. The phase of the MRGWs wave tilts eastward with height, from 700 hPa
 131 to 200 hPa, i.e., in the troposphere, while the phase tend to tilt westward from the upper troposphere to the lower stratosphere
 132 (Holton, 1979; Yang and Hoskins, 2017) reflecting the vertical structure of these equatorial waves.





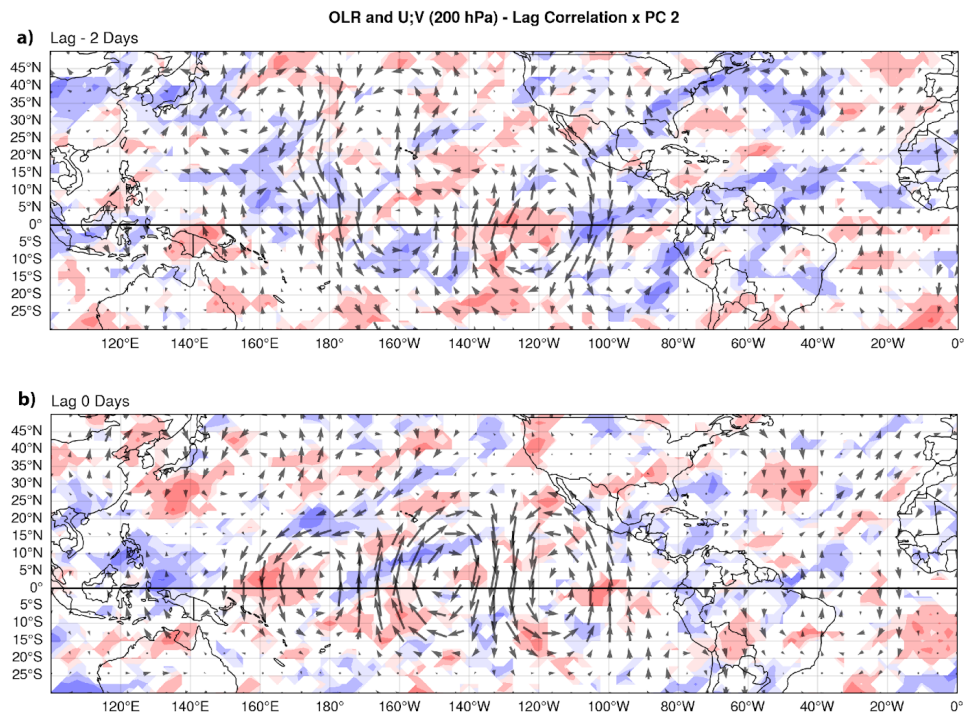
134

135

136 **Figure 2: Composite patterns based on PC1 > 1 conditions, showing band-pass filtered wind anomalies (3–8 day periods) at (a) 200**
 137 **hPa, (b) 500 hPa and (c) 700 hPa. Wind anomalies are depicted as vectors, with dashed lines indicating convergence and solid lines**
 138 **showing divergence. Shading represents band-passed filtered anomalies of outgoing longwave radiation (OLR) (red and blue) and**
 139 **band-passed filtered specific humidity (brown and green).**

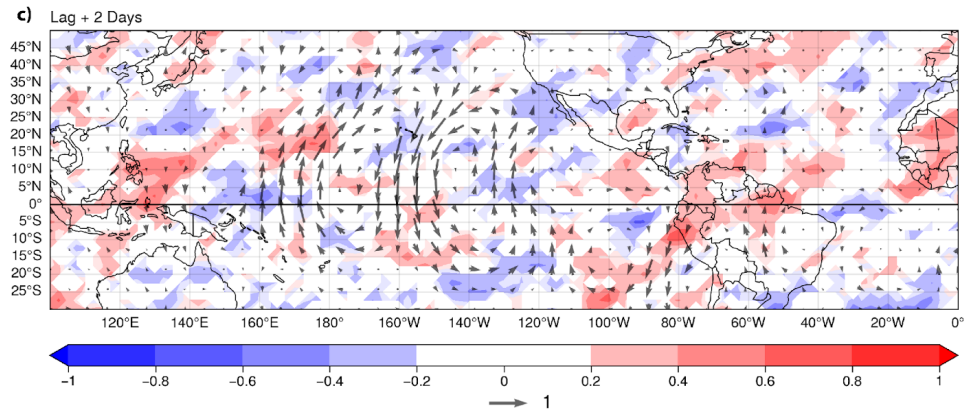
140 As MRGW evolves across the Pacific, the zones of convergence and divergence move westward along with the
 141 corresponding convective activity anomalies. The temporal evolution of a MRGW wind field and the associated tropical
 142 convection anomalies may be analyzed by examining the sequence of events, from the onset of the equatorial wave around
 143 200 hPa, to a few days later, when its signal is observed at lower tropospheric levels. One point lag correlations between PC2
 144 and unfiltered anomalies of 200 hPa wind and unfiltered OLR anomalies, for the -2 days to +2 days range, show the
 145 evolution of a MRGW with an approximate 4 to 5 days period. The vector represents the magnitude of the correlations
 146 between PC2 and the zonal and meridional components of the anomalous wind field. At lag -2 days, the correlation with the
 147 wind field shows the MRGW pattern over the central eastern Pacific with vortices between 20°N and 20°S. In the central
 148 eastern an anticyclonic equatorial circulation is connected to a midlatitude wave that emanates from the northwest Pacific
 149 (Fig.3.a). The cyclonic circulation in midlatitudes mechanically couples with the MRGW that extends across the Pacific, in a
 150 similar manner as laterally forced MRGWs presented by Magaña and Yanai (1995); Kiladis et al. (2016); Suhas et al. (2020)
 151 and Shreya and Suhas (2024). Over the central Pacific, negative (positive) OLR correlations (anomalies) are observed

152 between the clockwise and anticlockwise circulations of the MRGW over the equatorial region. In the early stages of the
153 MRGW, the OLR anomalies in the central Pacific are modulated by the midlatitude wave train, following the ascending and
154 descending motions described by the omega equation, i.e., negative OLR occurs ahead of troughs. However, at lag 0 days,
155 the MRGW propagates westward along with the antisymmetric anomalies in OLR around the dateline (Fig.3.b), with a
156 westward phase velocity of approximately $15 \text{ m}\cdot\text{s}^{-1}$ and a zonal wavenumber 5. The midlatitude wave propagates across the
157 eastern tropical Pacific, extending to the Southern Hemisphere to the western coast of South America (e.g. Braga et al.,
158 2022). At lag+2 days, the regions of convergence and divergence off the equator, around $15\text{-}20^\circ$ in latitude, displace
159 westward along with the tropical convection anomalies of the MRGW (Fig.3.c). At this stage the midlatitude wave train
160 weakens but the MRGW remains and is present over the westerly duct region, close to the western Pacific.



161

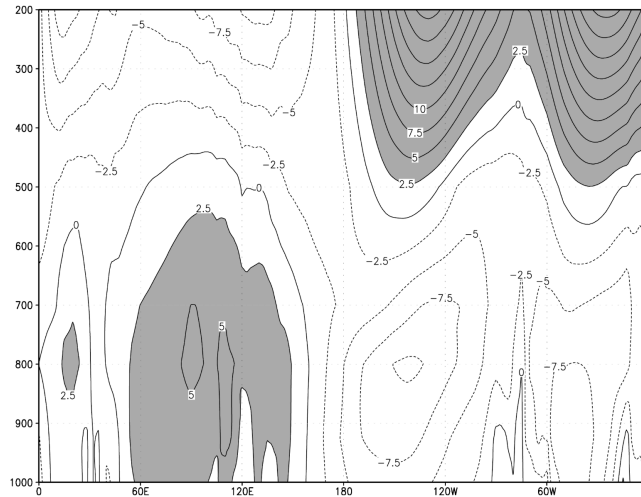
162



163

164 **Figure 3: Lag-cross correlation between the PC2 and the wind field anomalies at 200 hPa (vectors) and OLR anomalies (shades of**
 165 **red and blue), for the December–February period. Panels show results for: a) lag = -2 days, b) for lag= 0 days, and c) for lag = +2**
 166 **days. The correlations are calculated with unfiltered anomalies. A vector of magnitude 1 implies a perfect correlation.**

167 The maximum amplitude of MRGWs at upper levels occurs over the westerly duct region at 200 hPa, but its amplitude
 168 decreases over the Western Pacific, i.e., over a region with predominant easterly flow at upper tropospheric levels (Fig. 4).
 169 At lower tropospheric levels though, the westerly flow is observed over the western Pacific, where MRGWs have been
 170 documented around 850hPa (Kiladis et al., 2009). In this region, lower tropospheric MRGWs are better defined and may
 171 even lead to the formation of tropical cyclones (Dickinson and Molinari, 2002; Zhou and Wang, 2007).

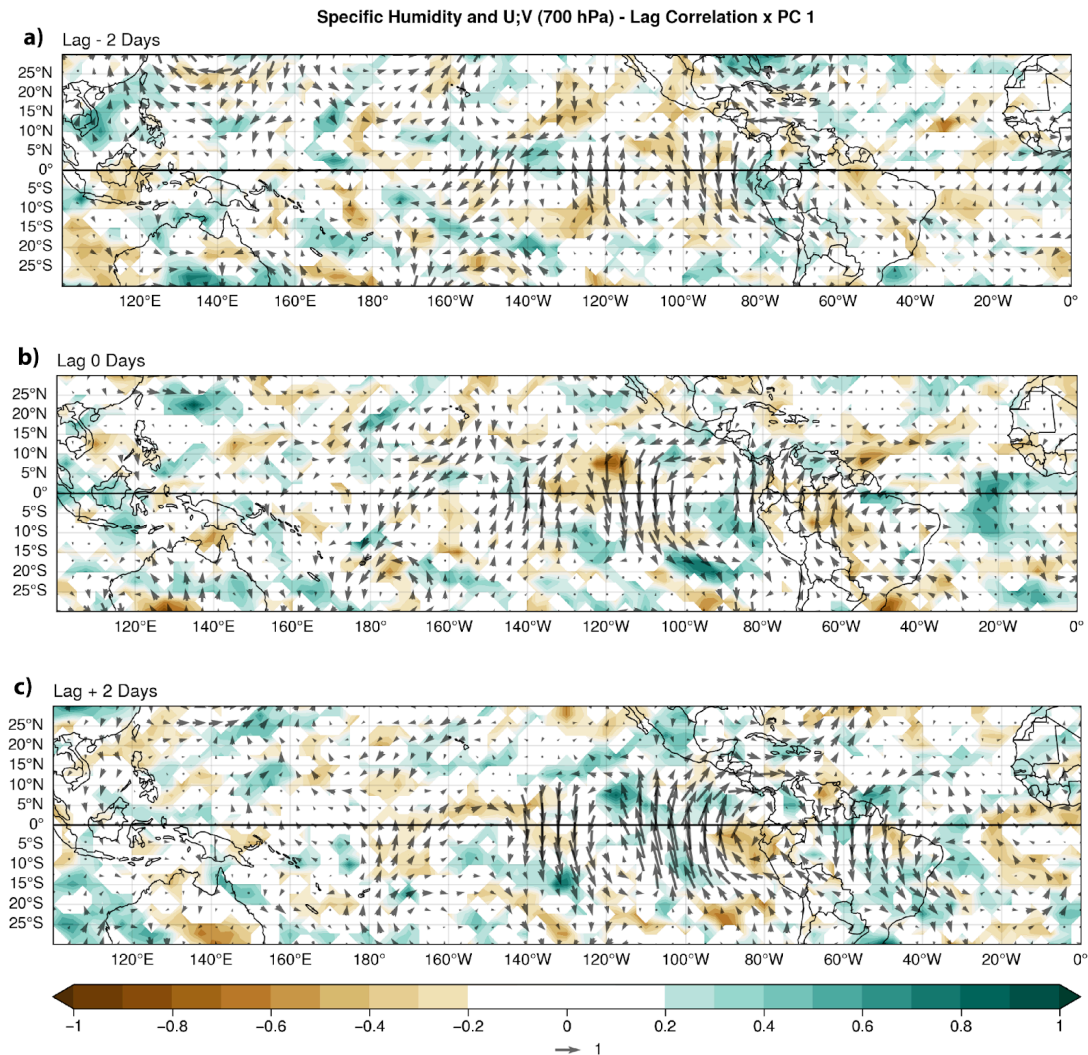


172

173 **Figure 4: Vertical cross section of the climatological zonal wind ($\text{m}\cdot\text{s}^{-1}$) along the equator between December and February**
 174 **1991-2020. Shading corresponds to regions of westerlies.**

175 In the central eastern Pacific, MRGW activity is an important mechanism to modulate the lower tropospheric moisture field
 176 that results in tropical convection. Lagged cross correlations between PC1 and 700 hPa wind field and anomalies of 700 hPa
 177 specific humidity show that MRGW modulate atmospheric moisture near the boundary layer. At lag -2 days, the clockwise

178 and anticlockwise vortices tend to modulate the antisymmetric response in specific humidity over the eastern Pacific, around
 179 100°W (Fig.5.a). At lag 0 days, the MRGW signal extends from the central Pacific into the western equatorial Atlantic, and
 180 the antisymmetric atmospheric moisture anomalies are observed in the corresponding divergent and convergent regions off
 181 the equator, between 5° and 10° in latitude and around 100°-120°W (Fig.5.b). This equatorial disturbance exhibits a dominant
 182 zonal wavenumber 5 structure and its evolution into the Atlantic is in agreement with the eastward group velocity associated
 183 with MRGWs. At lag +2 days, the signal in specific humidity correlations moves westward, maintaining the antisymmetric
 184 structure off the equator and extending to the Atlantic Ocean (Fig.5.c). The signal of the MRGW extends to the equatorial
 185 Atlantic and there are some signals of the modulation in the specific humidity field due to the eastward group velocity.



186

187

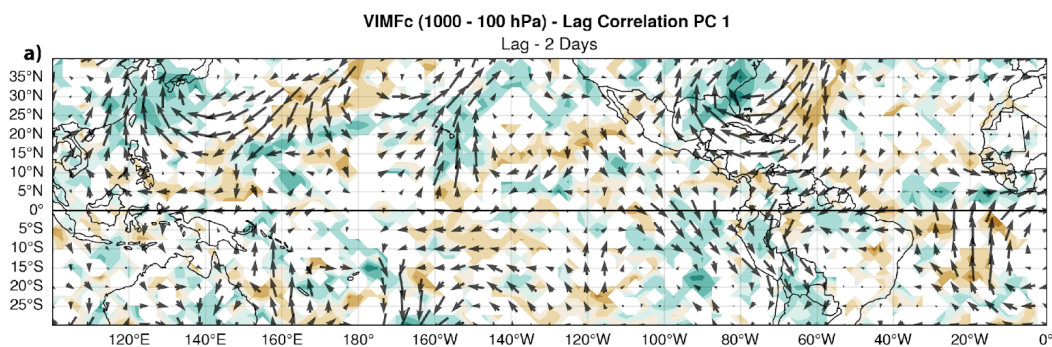
188

189 **Figure 5:** Lag-cross correlation between the first principal component (PC1) and the 700 hPa anomalous wind field (vectors) and
 190 700 hPa specific humidity (shades of green and brown), for the December–February period. Panels show results for: a) lag = -2

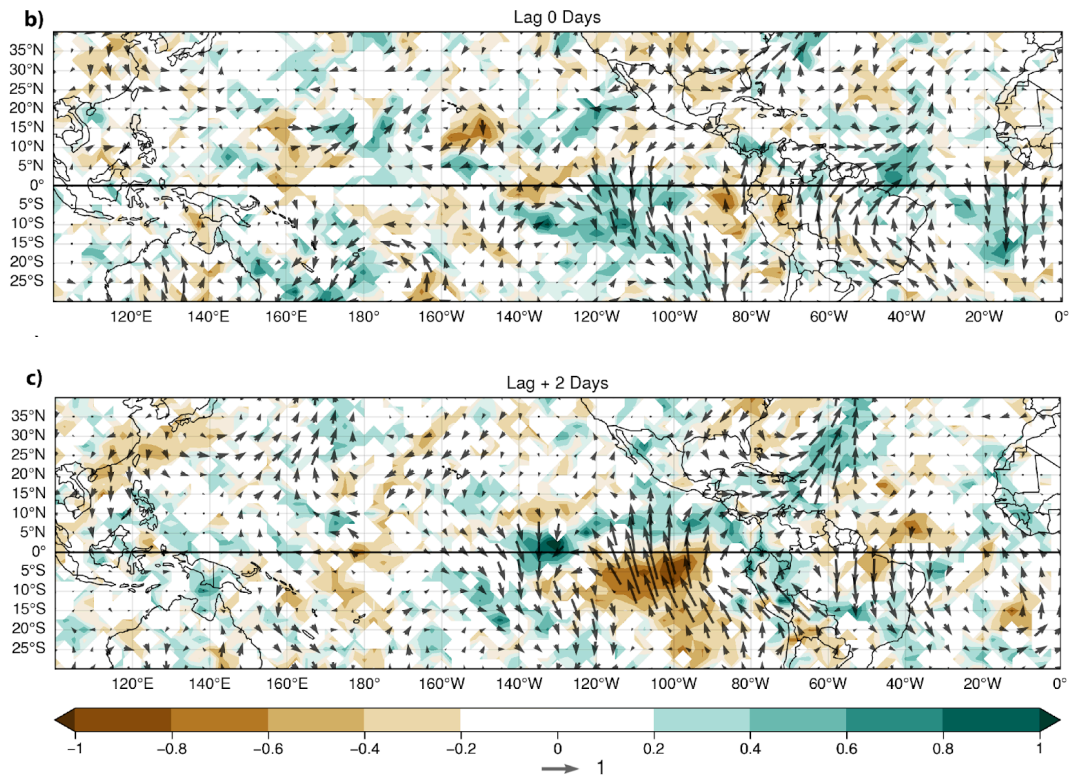
191 days, b) lag = 0 days, and c) lag = +2 days. The correlations are calculated with unfiltered anomalies. A vector of magnitude 1
192 implies a perfect correlation.

193 3.2 Vertically Integrated Moisture Flux in the tropics

194 The modulation of moisture by low level MRGW circulations is diagnosed by examining the Vertically Integrated Moisture
195 Flux (VIMF) and its convergence. As previously stated, VIMF is a measure of the amount of water vapor transported in the
196 atmosphere and its convergence is used to determine zones of intense convective activity. The lagged correlations of PC1
197 and VIMF and its convergence show that a MRGW tends to create regions of moisture accumulation that result in tropical
198 convective activity. By lag -2 days, the signals of a MRGW along the eastern equatorial Pacific and a midlatitude wave from
199 the northern subtropics, around the westerly duct region, exhibits the tropical-midlatitude interaction signal that leads to the
200 formation of a MRGW (Fig.6.a). The positive and negative vertical motion anomalies reflect in the regions of VIMF
201 convergence and divergence in the midlatitude wave. In the equatorial region, moisture convergence and divergence are
202 located off the equator as expected in a MRGW. At lag 0 days, VIMF and its convergence-divergence zones show the
203 westward movement of the MRGW and the antisymmetric location of the associated zones of moisture convergence and
204 divergence (Fig.6.b). The spatial structure of VIMF correlations approximately match the one observed for the wind field
205 anomalies at 700 hPa (see Fig.5.b) indicating that VIMF is capturing the signal of MRGW at lower tropospheric levels. Such
206 anomalous circulation modulates zones of specific humidity anomalies off the equator in the central-eastern equatorial
207 Pacific. By lag +2 days, the MRGW signal shows that moisture convergence and divergence are asymmetrically distributed
208 (Fig.6.c), contributing to increases and decreases of specific humidity between 150°W and 70°W. The previous analysis
209 shows that moisture is controlled by the MRGW at lower tropospheric levels inducing zones of negative and positive
210 convective activity anomalies. The quadrature between the phase of the MRGW at upper and lower tropospheric levels
211 serves to connect moisture convergence (divergence) at 700 hPa with divergence (convergence) at 200 hPa, characteristics of
212 deep tropical convective systems.



213

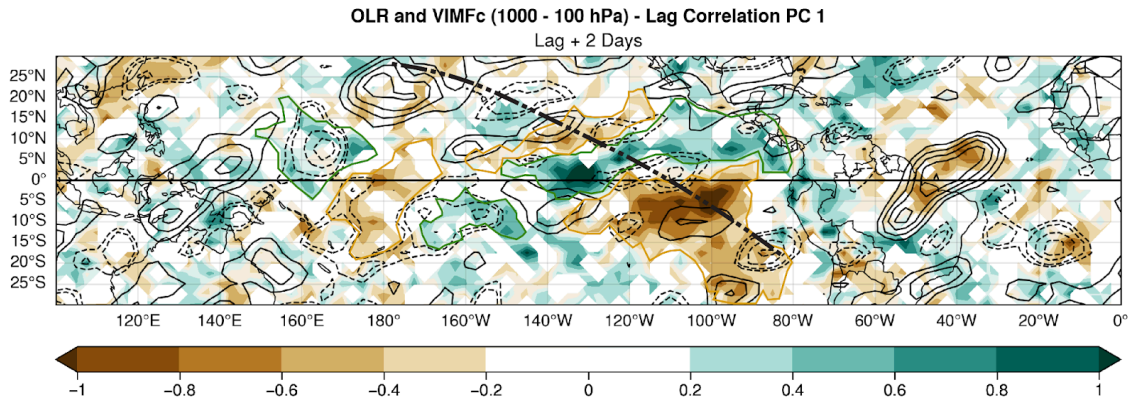


214

215

216 **Figure 6: Lag-cross correlation between the first principal component (PC1) and VIMF anomalies (vectors) and VIMF**
 217 **convergence (shades of green) and VIMF divergence (shades of brown) anomalies for the December – February months. a) lag = -2**
 218 **days, b) lag = 0 days, and c) lag = +2 days. The correlations are calculated with unfiltered anomalies. A vector of magnitude 1**
 219 **implies a perfect correlation.**

220 The relationship between VIMF convergence-divergence anomalies and OLR anomalies may be shown by means of the lag
 221 correlations between PC1 and VIMF convergence and OLR anomalies. For brevity, this relationship is shown only for lag +2
 222 days (Fig.7). The signal of a midlatitude wave approaching the westerly duct region is observed as positive and negative
 223 correlations corresponding to VIMF convergence (divergence) and OLR negative (positive) anomalies. The signal extends
 224 into South America showing that the mid latitude wave not only triggers a MRGW, but it also continues its interhemispheric
 225 propagation (Webster and Holton, 1982; Tomas and Webster, 1994; Li et al., 2015; Kiladis et al., 2016; Braga et al., 2022;
 226 Braga et al., 2024). Along the equatorial region the antisymmetric signals in correlation appear for VIMF convergence
 227 (divergence) and OLR anomalies extending from 180° to 80°W.



228

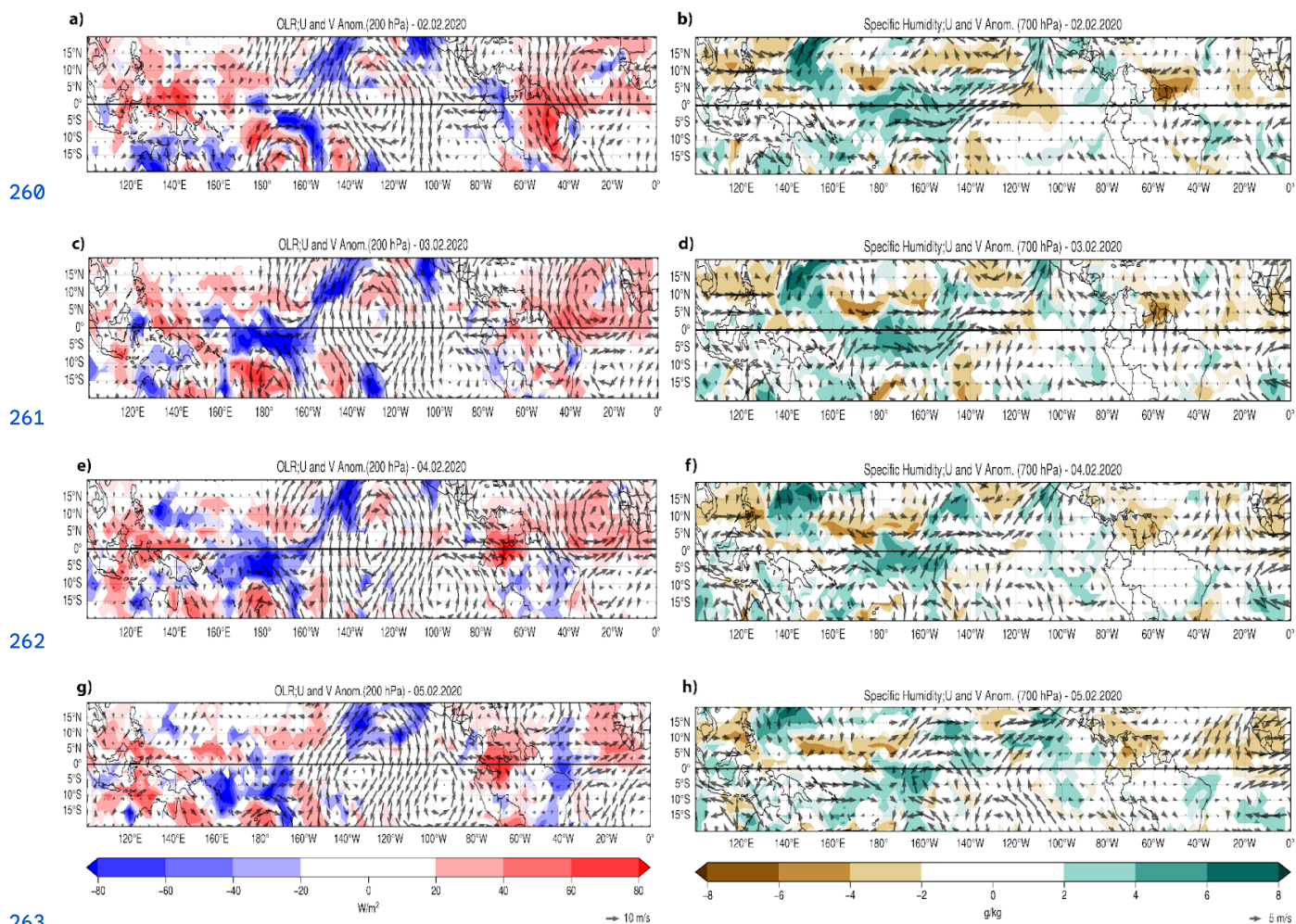
229 **Figure 7: Lagged +2 days correlation between the first principal component (PC1) and OLR and VIMFc unfiltered anomalies.**
 230 **OLR correlations are represented by solid lines (positive) and dashed lines (negative), while VIMF convergence is shown in shades**
 231 **of green and divergence in shades of brown. The thick dashed-dotted line indicates the trajectory of the mid-latitude wave. The**
 232 **brown and green lines highlight the zone of antisymmetric VIMFc in the MRGW.**

233 Over the northeastern subtropical Pacific, the interaction between the midlatitude wave and the MRGW VIMF convergence
 234 induces a moisture plume that at times results in precipitation events over México (Fig.7). The structure of such a moisture
 235 plume approximately corresponds to the so-called tropical plumes described by Knippertz (2007) and Fröhlich et al. (2013).

236 3.3 Case Study

237 The presence of MRGWs in the daily atmospheric circulations in upper and lower tropospheric levels is obtained for
 238 absolute values of PC1 larger than 1.0, as in February 2–6, 2020. On February 2, 2020, a midlatitude wave at upper
 239 tropospheric levels over the central-northeastern Pacific propagates into the tropics across the westerly duct region, coupled
 240 with the characteristic circulation of a MRGW around 180°W. At 200 hPa (180°W-120°W) OLR positive and negative
 241 anomalies are observed in the regions of ascending and descending motions associated with the midlatitude wave that
 242 propagates from the Northern to the Southern Hemisphere (Fig.8.a). The clockwise equatorial circulation at 200 hPa
 243 corresponds to part of the midlatitude wave but it is also a characteristic of the equatorial MRGW. At lower tropospheric
 244 levels (700 hPa), there is only a slight signal of this clockwise circulation, almost in phase with the upper tropospheric
 245 vortex. At this level as well, the midlatitude wave is hardly present in the wind field around the subtropics, but it shows
 246 negative and positive specific humidity anomalies in the convergence and divergence regions around 20°N (Fig.8.b). By
 247 February 3, 2020, the midlatitude wave at 200 hPa extends to the Pacific coast of South America with the corresponding
 248 positive and negative anomalies in OLR (Fig.8.c). At around 130°W, a well-defined vortex corresponds to an equatorial
 249 clockwise circulation with antisymmetric OLR anomalies. At 700 hPa, a clockwise circulation may also be identified at
 250 140°W, with signals of a vortex that corresponds to the MRGW with positive and negative specific humidity anomalies
 251 around (Fig.8.d). By February 4, 2020, the mid latitude wave in the Northern Hemisphere subtropics remains, but it
 252 intensifies in the equatorial and the tropical Southern Hemisphere region (Fig.8.e). In the lower troposphere the clockwise

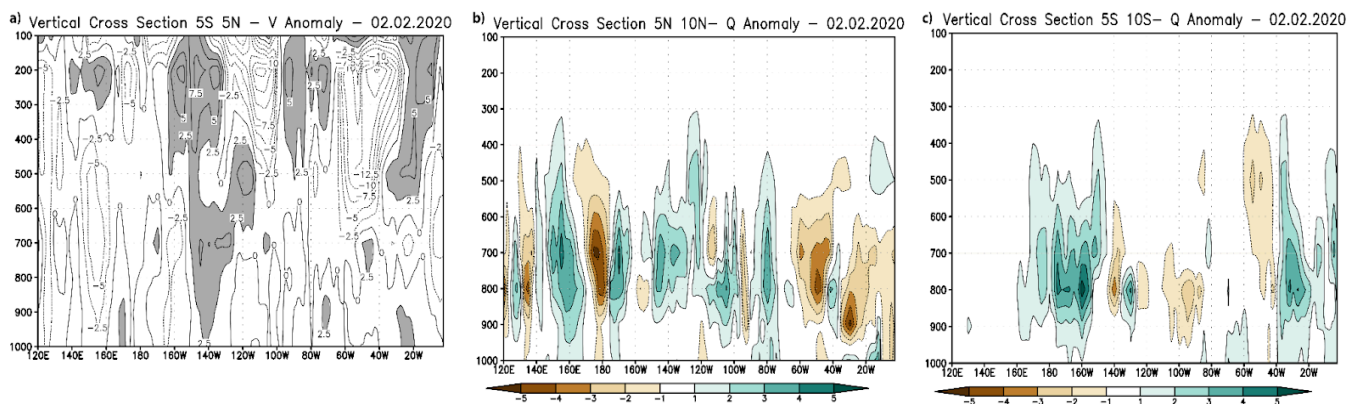
253 circulation in the equatorial region is better defined and the anti-symmetric structure in the surrounding specific humidity
 254 anomalies, characteristic of the MRGW, begins to form between 180°W and 140°W (Fig.8.f). On February 5, 2020, the
 255 MRGW began its westward movement with anti-symmetric OLR anomalies better defined on its westward side. The
 256 midlatitude wave signal in the north-central Pacific weakens (Fig.8.g). At lower levels the clockwise circulation associated
 257 with the MRGW is well defined over the equator and shows a westward displacement with the specific humidity anomalies
 258 anti-symmetrically distributed around this circulation, in the moisture convergent and divergent regions (Fig.8.h). The
 259 structure of the MRGW at 700 hPa appears to be better defined as it approaches the westerly winds, west of the dateline.



264 **Figure 8: 200 hPa unfiltered wind anomalies and unfiltered OLR anomalies (left column, 700 hPa unfiltered wind field and**
 265 **unfiltered specific humidity anomalies (right column) from February 2, 2020 to February 5, 2020: (a) and (b) for February 2, (c)**
 266 **and (d) for February 3, (e) and (f) for February 4, and (g) and (h) for February 5.**

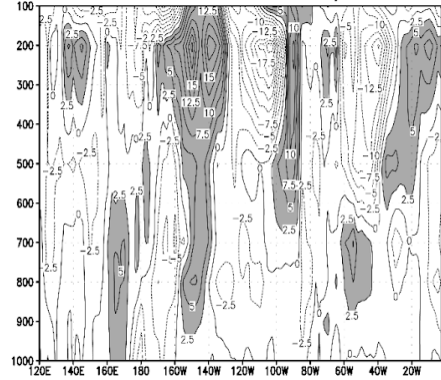
267 As observed by Zhou and Wang (2007) in their case study, a MRGW is triggered at upper tropospheric levels and its signal
 268 propagates downward in the following days. The sequence of atmospheric circulations between 02-05 February 2020 shows

269 that the equatorial wave circulations are well defined in the early days at 200 hPa, and its presence is better detected at later
 270 stages at 700 hPa. A vertical cross section of the meridional wind anomalies along the equator and specific humidity
 271 anomalies north and south of the equator (5°N-5°S) reflect the development of the vertical structure of the MRGW. The
 272 vertical cross section of the meridional wind anomalies between 5°S and 5°N (Fig.9.a) and specific humidity anomalies
 273 between 5°S and 10°S (Fig.9.b) and 5°N and 10°N (Fig.9.c), for February 2, 2020, shows that the signal of the MRGW in the
 274 wind field is present mainly at 200 hPa around 160°W-100°W, with magnitude of around $15 \text{ m}\cdot\text{s}^{-1}$, between 100 and 400 hPa.
 275 At this stage of development, the specific humidity anomalies do not appear to correspond to the moisture convergence and
 276 divergence induced by a MRGW. By February 3, 2020, the signal of the MRGW in the central eastern Pacific, at upper
 277 tropospheric levels, extends downward to around 700 hPa (Fig.9.d). Some indications of the induced effect of the lower
 278 tropospheric part of the MRGW show in the specific humidity, with positive-negative anomalies around 700 hPa, between
 279 160°E and 140°W (Fig.9.e). South of the equator the sign of these anomalies tends to be the opposite to its northward
 280 counterpart, but still is not well defined (Fig.9.f). By February 4, 2020, the quadrature in the anomalies of the meridional
 281 component of the wind field shows and extends to lower tropospheric levels with an eastward tilt with height at around
 282 150°W (Fig.9.g). The tilt with height approximately corresponds to a vertical wavelength of around 15 km, which
 283 approximately agrees with early estimates by Yanai and Hayashi (1969). At around 700 hPa positive and negative anomalies
 284 appear induced by moisture convergence and divergence associated with the MRGW (Fig.9.h and Fig.9.i). On February 5,
 285 2020, the structure of the MRGW in the troposphere exhibits the tilt with height associated with the vertical wavelength
 286 between 180°W and 120°W (Fig.9.j). North and south of the equator, antisymmetric anomalies in the specific humidity field
 287 are well defined in association with the circulations induced by the MRGW (Fig.9.k. and Fig.9.l). This case study suggests
 288 that the moisture anomalies in the lower tropospheric levels tend to develop as the MRGW propagates downward from the
 289 upper tropospheric levels where it was triggered by a midlatitude wave. Once MRGW is well developed, it modulates
 290 moisture convergence and develops as deep convection due to the wind divergence in the upper troposphere.



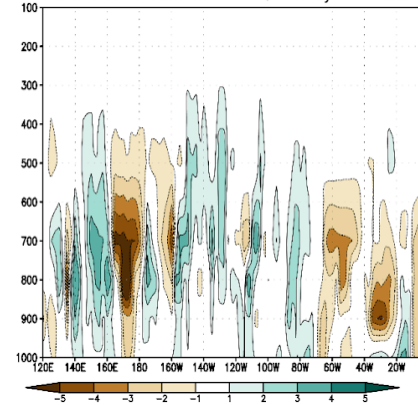
291

d) Vertical Cross Section 5S 5N – V Anomaly – 03.02.2020

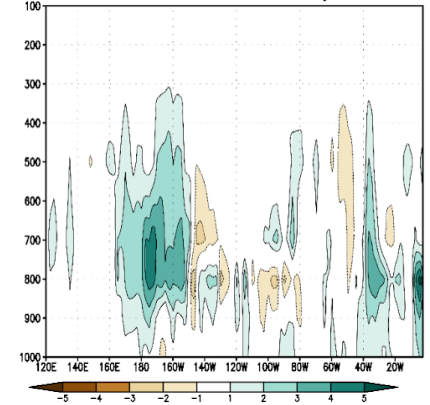


292

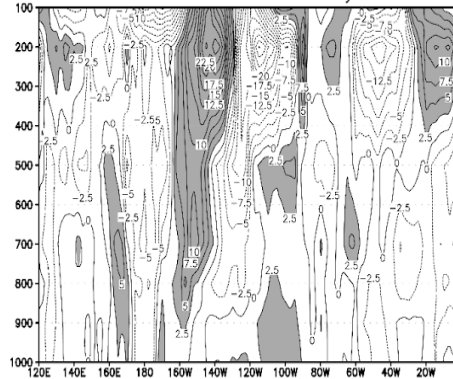
e) Vertical Cross Section 5N 10N– Q Anomaly – 03.02.2020



f) Vertical Cross Section 5S 10S– Q Anomaly – 03.02.2020

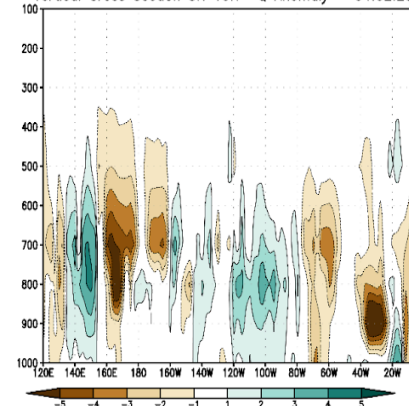


g) Vertical Cross Section 5S 5N – V Anomaly – 04.02.2020

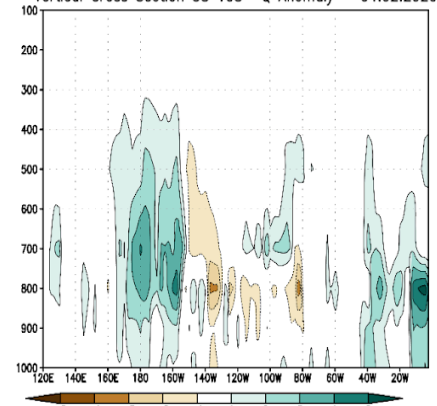


293

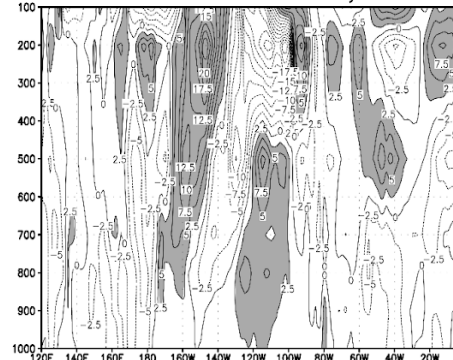
h) Vertical Cross Section 5N 10N– Q Anomaly – 04.02.2020



i) Vertical Cross Section 5S 10S– Q Anomaly – 04.02.2020

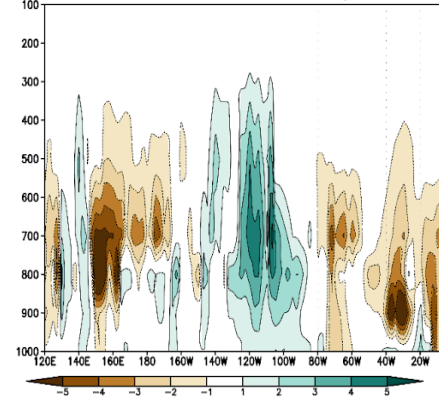


j) Vertical Cross Section 5S 5N – V Anomaly – 05.02.2020

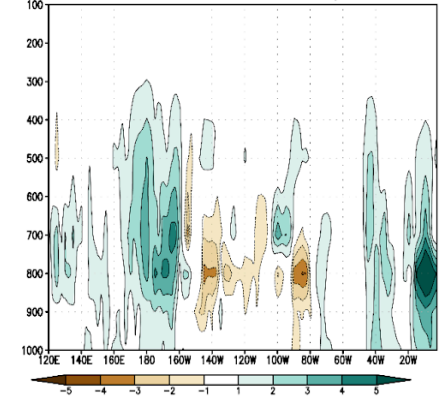


294

k) Vertical Cross Section 5N 10N– Q Anomaly – 05.02.2020



l) Vertical Cross Section 5S 10S– Q Anomaly – 05.02.2020



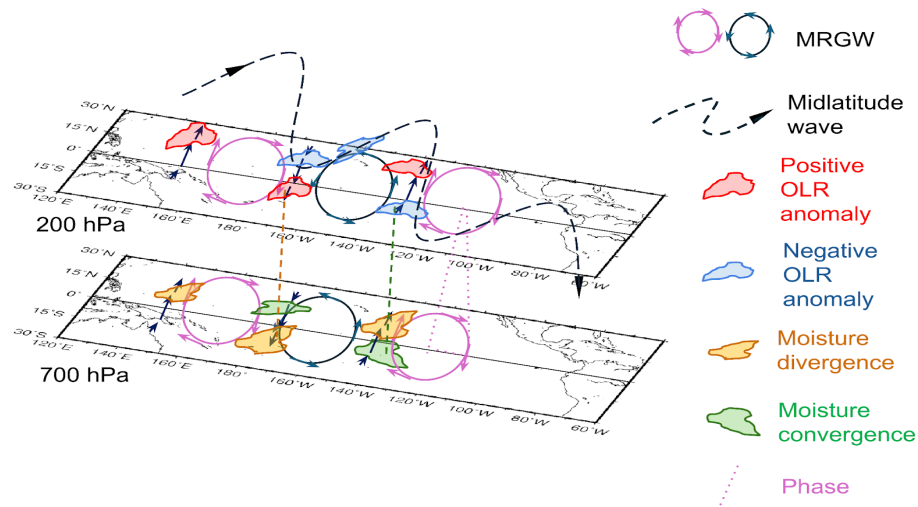
295 Figure 9: Vertical cross-sections (longitude – height) (1000–100 hPa, between 5°S–5°N) for daily unfiltered meridional wind
296 anomalies (left column) and daily unfiltered specific humidity anomalies (central and right columns) from February 2 to 5, 2020:
297 (a), (b), and (c) for February 2; (d), (e), and (f) for February 3; (g), (h), and (i) for February 4; and (j), (k), and (l) for February 5.

298 These results are like those of Zhou and Wang (2007) and indicate a change in the wavelength of the MRGW as the signal
299 propagates from the upper tropospheric levels over the western Pacific. As the MRGW signal propagates downward and
300 westward into the western Pacific, the wavelength appears to decrease from a dominant wavenumber 5 to a zonal
301 wavenumber 6. The change from easterlies to westerlies appears to affect the propagation and energetics of the MRGW at
302 lower tropospheric levels (Webster and Chang, 1988) and may influence the change in the spatial structure of the MRGW at
303 lower tropospheric levels.

304 4. Summary and Conclusions

305 Upon the discovery of equatorial waves, numerous studies have proposed that they are forced either by a midlatitude wave
306 propagating into the tropics, or by convective activity near the equatorial regions. Lateral forcing appears to be the most
307 frequently accepted triggering mechanism for MRGW (Magaña and Yanai, 1995; Zhou and Wang, 2007; Suhas et al., 2020;
308 Shreya and Suhas, 2024). However, there is still some debate on the relationship between MRGW and tropical convective
309 activity. Even more, the signals of MRGW in the upper and lower troposphere are often treated separately.

310 The present study shows a plausible explanation to coherently relate all these elements considering forcing of equatorial
311 circulation with the characteristics of a MRGW by a midlatitude wave that propagates across the westerly duct region. As
312 suggested by Au-Yeung and Tam (2018), the MRGW extends to from the upper, where it is initiated, to the lower
313 troposphere levels, where it changes the atmospheric moisture field, resulting in antisymmetric anomalies in specific
314 humidity off the equator, as those reported in other observational analyses (e.g. Kiladis et al., 2009). The phase difference
315 (quadrature) between the upper tropospheric MRGW circulations (wind convergence-divergence) and its lower tropospheric
316 counterpart (moisture divergence-convergence) reinforce the development of deep tropical convection that shows as positive
317 and negative OLR anomalies off the equator (Fig.10). Therefore, a key element to associate convective activity and
318 atmospheric circulation in a MRGW is the eastward tilt with height in the troposphere that results in a quadrature of the
319 phase of the wave. From the top of the troposphere to the stratosphere the westward tilt with height corresponds to the
320 vertical structure of the MRGW (e.g Holton, 1979; Yang and Hoskins, 2017).



321

322 **Figure 10: Schematic representation of the vertical structure of a MRGW and the corresponding circulation anomalies in the**
 323 **lower and upper tropospheric levels along with moisture and convective activity anomalies in divergent and convergent regions**
 324 **(vectors) of the wave. The dashed wavy line corresponds to the mid latitude wave in the upper troposphere.**

325 The development of MRGW constitutes a process that involves tropical midlatitude interactions that are of relevance for
 326 weather in the tropical region, where moisture convergence in the eastern tropical Pacific induced by MRGW constitute the
 327 source of convective activity, even for tropical plumes observed over Mexico during the boreal winter season (Knippertz,
 328 2007; Fröhlich et al., 2013). In addition, the propagation of the midlatitude wave into the Southern Hemisphere through the
 329 westerly duct affects weather over South America (Braga et al., 2022).

330 Thanks to the improvement of atmospheric reanalysis, it is now possible to more accurately describe the characteristics of
 331 equatorial waves in the troposphere and even in the stratosphere. A systematic identification of equatorial wave activity may
 332 serve to better define the influence of these systems in weather in several tropical regions, for instance in the tropical
 333 Americas. In summary, a key element of tropical weather in the eastern Pacific are MRGWs and consequently, a better
 334 understanding of the processes of modulation of atmospheric moisture and convective activity may significantly improve
 335 weather forecasts in the tropical and subtropical regions.

336

337 **Author Declaration**

338 **Funding information:** This work was supported by UNAM Postdoctoral Program (POSDOC) - DGPA 13189. Victor
 339 Magaña. was financially supported by the CONAHCYT Grant PCC-319779.

340 **Conflicts of interest:** There is no conflict of interest.

341 **Ethics approval:** All authors have approved this manuscript.

342 **Consent to participate:** All authors have provided their consent to submit this manuscript to Weather and Climate
 343 Dynamics.

344 **Consent for publication:** All authors give permission to publish this manuscript.

345 **Data availability:** Publicly available datasets were analyzed in this study. This data can be found here:

346 <https://www.ecmwf.int/en/forecasts/dataset/ecmwf-reanalysis-v5>.

347 **Authors' contributions:** Hugo A. Braga analyzed the data, wrote the manuscript, and prepared the figures. Victor Magaña
348 contributed some parts and reviewed the manuscript together with the first author.

349 **Acknowledgements:** We are grateful to the Departamento de Geografía Física at the Instituto de Geografía, UNAM, for
350 their valuable support. Special thanks to Gustavo Vázquez for his outstanding technical assistance. This project was made
351 possible through the DGAPA-UNAM postdoctoral fellowship (Grant 13189) and the CONAHCYT Grant PCC-319779. We
352 sincerely thank Dr. George Kiladis and the anonymous reviewer for their constructive comments and suggestions, which
353 have significantly improved the manuscript.

354 **References**

355 Au-Yeung, A. Y. M., and C.-Y. Tam: Dispersion characteristics and circulation associated with boreal summer
356 westward-traveling mixed Rossby–gravity wave–like disturbances, *J. Atmos. Sci.*, 75(2), 513–533,
357 <https://doi.org/10.1175/JAS-D-16-0245.1>, 2018.

358 Bennet, J.R., and J.A. Young: The influence of latitudinal with shear upon large-scale wave propagation into the tropics,
359 *Mon. Wea. Rev.*, 99, 201–214, https://doi.org/10.2151/jmsj1965.52.3_261,1971.

360 Braga, H. A., Ambrizzi, T., and N. M. J. Hall: Relationship between interhemispheric Rossby wave propagation and South
361 Atlantic Convergence Zone during La Niña years, *Int. J. Climatol.*, 13, <https://doi.org/10.1002/joc.7755>, 2022.

362 Braga, H.A., Ambrizzi, T., and N. M. J. Hall: South Atlantic Convergence Zone as Rossby wave source, *Theor. Appl.*
363 *Climatol.*, 155, 4231–4247, <https://doi.org/10.1007/s00704-024-04877-y>, 2024.

364 Dickinson, M., and J. Molinari: Mixed Rossby–Gravity Waves and Western Pacific Tropical Cyclogenesis. Part I: Synoptic
365 Evolution, *J. Atmos. Sci.*, 59, 2183–2196, [https://doi.org/10.1175/1520-0469\(2002\)059<2183>2.0.CO;2](https://doi.org/10.1175/1520-0469(2002)059<2183>2.0.CO;2), 2002.

366 Duchon, C. E.: Lanczos filtering in one and two dimensions, *J. Appl. Meteor. Climatol.*, 18(8), 1016–1022,
367 [https://doi.org/10.1175/1520-0450\(1979\)018<1016>2.0.CO;2](https://doi.org/10.1175/1520-0450(1979)018<1016>2.0.CO;2), 1979.

368 Fasullo, J., and P. J. Webster: A hydrological definition of Indian monsoon onset and withdrawal, *J. Clim.*, 16(19),
369 3200–3211, [https://doi.org/10.1175/1520-0442\(2003\)016<3200>2.0.CO;2](https://doi.org/10.1175/1520-0442(2003)016<3200>2.0.CO;2), 2003.

370 Fröhlich, L., P. Knippertz, A. H. Fink, and E. Hohberger: An objective climatology of tropical plumes, *J. Clim.*, 26,
371 5044–5060, <https://doi.org/10.1175/JCLI-D-12-00351.1>, 2013.

372 Hayashi, Y.: A theory of large-scale equatorial waves generated by condensation heat and accelerating, *J. Meteor. Soc. Jpn.*
373 *Ser. II*, 48(2), 140–160, https://doi.org/10.2151/jmsj1965.48.2_140, 1970.

374 Hayashi, Y.: Interpretations of space-time spectral energy equations, *J. Atmos. Sci.*, 39(3), 685–688,
375 [https://doi.org/10.1175/1520-0469\(1982\)039<0685>2.0.CO;2](https://doi.org/10.1175/1520-0469(1982)039<0685>2.0.CO;2), 1982.

376 Hayashi, Y., and D. G. Golder: The generation of equatorial transient planetary waves: Control experiments with a GFDL
377 general circulation model, *J. Atmos. Sci.*, 35(11), 2068–2082, [https://doi.org/10.1175/1520-0469\(1978\)035<2068>2.0.CO;2](https://doi.org/10.1175/1520-0469(1978)035<2068>2.0.CO;2),
378 1978.

379 Hess, P., H. Hendon, and D. S. Battisti: The relationship between mixed Rossby gravity waves and convection in a general
380 circulation model, *J. Meteor. Soc. Jpn.*, 71, 321–338, 1993.

381 Hersbach, H., and Coauthors: The ERA5 global reanalysis, *Q. J. R. Meteorol. Soc.*, 146(730), 1999–2049,
382 <https://doi.org/10.1002/qj.3803>, 2020.

383 Holton, J. R.: Waves in the equatorial stratosphere generated by tropospheric heat sources, *J. Atmos. Sci.*, 29(2), 368–375,
384 [https://doi.org/10.1175/1520-0469\(1972\)029<0368>2.0.CO;2](https://doi.org/10.1175/1520-0469(1972)029<0368>2.0.CO;2), 1972.

385 Holton, J.R.: *An Introduction to Dynamic Meteorology*, Academic Press, New York, 391 pp., 1979.

386 Kiladis, G. N., M. C. Wheeler, P. T. Haertel, K. H. Straub, and P. E. Roundy: Convectively coupled equatorial waves, *Rev.*
387 *Geophys.*, 47(2), <https://doi.org/10.1029/2008RG000266>, 2009.

388 Kiladis, G. N., Dias, J., and Gehne, M.: The relationship between equatorial mixed Rossby–gravity and eastward
389 inertio-gravity waves. Part I, *J. Atmos. Sci.*, 73, 2123–2145, <https://doi.org/10.1175/JAS-D-15-0230.1>, 2016.

390 Knippertz, P.: Tropical–extratropical interactions related to upper-level troughs at low latitudes, *Dyn. Atmos. Oceans*,
391 43(1–2), 36–62, <https://doi.org/10.1016/j.dynatmoce.2006.06.003>, 2007.

392 Knippertz, P., Gehne, M., Kiladis, G. N., Kikuchi, K., Rasheeda Satheesh, A., Roundy, P. E., et al.: The intricacies of
393 identifying equatorial waves, *Q. J. R. Meteorol. Soc.*, 148(747), 2814–2852, <https://doi.org/10.1002/qj.4338>, 2022.

394 Li, Y., J. Li, F. F. Jin, and S. Zhao: Interhemispheric propagation of stationary Rossby waves in a horizontally nonuniform
395 background flow, *J. Atmos. Sci.*, 72(8), 3233–3256, <https://doi.org/10.1175/JAS-D-14-0239.1>, 2015.

396 Li, Y., J. Feng, J. Li, and A. Hu: Equatorial windows and barriers for stationary Rossby wave propagation, *J. Clim.*, 32,
397 6117–6135, <https://doi.org/10.1175/JCLI-D-18-0722.1>, 2019.

398 Liebmann, B., and C. A. Smith: Description of a complete (interpolated) outgoing longwave radiation dataset, *Bull. Am.*
399 *Meteor. Soc.*, 77(6), 1275–1277, <https://doi.org/10.2307/26233278>, 1996.

400 Magaña, V., and M. Yanai: Tropical-midlatitude interaction on the time scale of 30 to 60 days during the Northern summer of
401 1979, *J. Clim.*, 4, 180–201, [https://doi.org/10.1175/1520-0442\(1991\)004<0180>2.0.CO;2](https://doi.org/10.1175/1520-0442(1991)004<0180>2.0.CO;2), 1991.

402 Magaña, V., and M. Yanai: Mixed Rossby–gravity waves triggered by lateral forcing, *J. Atmos. Sci.*, 52(9), 1473–1486,
403 [https://doi.org/10.1175/1520-0469\(1995\)052<1473>2.0.CO;2](https://doi.org/10.1175/1520-0469(1995)052<1473>2.0.CO;2), 1995.

404 Mak, M.: Laterally driven stochastic motions in the tropics, *J. Atmos. Sci.*, 26, 41–64,
405 [https://doi.org/10.1175/1520-0469\(1969\)026<0041>2.0.CO;2](https://doi.org/10.1175/1520-0469(1969)026<0041>2.0.CO;2), 1969.

406 Maruyama, T.: Large-scale disturbances in the equatorial lower stratosphere, *J. Meteor. Soc. Jpn. Ser. II*, 45(5), 391–408,
407 https://doi.org/10.2151/jmsj1965.45.5_391, 1967.

408 Matsuno, T.: Quasi-geostrophic motions in the equatorial area, *J. Meteor. Soc. Jpn. Ser. II*, 44(1), 25–43,
409 https://doi.org/10.2151/jmsj1965.44.1_25, 1966.

410 Nitta, T.: Statistical study of tropospheric wave disturbances in the tropical Pacific region, *J. Meteor. Soc. Jpn. Ser. II*, 48(1),
411 47–60, https://doi.org/10.2151/jmsj1965.48.1_47, 1970.

412 Pazos, M., V. Magaña, and E. Herrera: Easterly wave activity in the Intra-Americas Seas region analyzed with vertically
413 integrated moisture fluxes, *Front. Earth Sci.*, 11, 1223939, <https://doi.org/10.3389/feart.2023.1223939>, 2023.

414 Suhas, E., Neena, J. M., and Jiang, X.: Exploring the factors influencing the strength and variability of convectively coupled
415 mixed Rossby–gravity waves, *J. Clim.*, 33, 9705–9719, <https://doi.org/10.1175/JCLI-D-20-0218.1>, 2020.

416 Shreya, K., and E. Suhas: A survey of westward-propagating mixed Rossby–Gravity waves and quantification of their
417 association with extratropical disturbances, *Q. J. R. Meteorol. Soc.*, 1–19, <https://doi.org/10.1002/qj.4668>, 2024.

418 Takayabu, N. Y., and T. Nitta: 3–5 day-period disturbances coupled with convection over the tropical Pacific Ocean, *J.*
419 *Meteor. Soc. Jpn.*, 71, 221–245, https://doi.org/10.2151/jmsj1965.71.2_221, 1993.

420 Tomas, R. A., and P. J. Webster: Horizontal and vertical structure of cross-equatorial wave propagation, *J. Atmos. Sci.*,
421 51(11), 1417–1430, [https://doi.org/10.1175/1520-0469\(1994\)051<1417>2.0.CO;2](https://doi.org/10.1175/1520-0469(1994)051<1417>2.0.CO;2), 1994.

422 Webster, P. J., and J. R. Holton: Cross-equatorial response to middle-latitude forcing in a zonally varying basic state, *J.*
423 *Atmos. Sci.*, 39(4), 722–733, [https://doi.org/10.1175/1520-0469\(1982\)039<0722>2.0.CO;2](https://doi.org/10.1175/1520-0469(1982)039<0722>2.0.CO;2), 1982.

424 Webster, P. J., and H. Chang: Equatorial energy accumulation and emanation regions: Impacts of a zonally varying basic
425 state, *J. Atmos. Sci.*, 45, 803–829, [https://doi.org/10.1175/1520-0469\(1988\)045<0803:EEAAER>2.0.CO;2](https://doi.org/10.1175/1520-0469(1988)045<0803:EEAAER>2.0.CO;2), 1988.

426 Wheeler, M., and G. N. Kiladis: Convectively coupled equatorial waves: Analysis of clouds and temperature in the
427 wavenumber–frequency domain, *J. Atmos. Sci.*, 56, 374–399, [https://doi.org/10.1175/1520-0469\(1999\)056<0374>2.0.CO;2](https://doi.org/10.1175/1520-0469(1999)056<0374>2.0.CO;2),
428 1999.

429 Yanai, M., and Y. Hayashi: Large-scale equatorial waves penetrating from the upper troposphere into the lower stratosphere,
430 *J. Meteor. Soc. Jpn. Ser. II*, 47(3), 167–182, https://doi.org/10.2151/jmsj1965.47.3_167, 1969.

431 Yanai, M., and T. Maruyama: Stratospheric wave disturbances propagating over the equatorial Pacific, *J. Meteor. Soc. Jpn.*
432 *Ser. II*, 44(5), 291–294, https://doi.org/10.2151/jmsj1965.44.5_291, 1966.

433 Yanai, M., and M. Murakami: A further study of tropical wave disturbances by the use of spectrum analysis, *J. Meteor. Soc.*
434 *Jpn. Ser. II*, 48(3), 185–197, https://doi.org/10.2151/jmsj1965.48.3_185, 1970a.

435 Yanai, M., and M. Murakami: Spectrum analysis of symmetric and antisymmetric equatorial waves, *J. Meteor. Soc. Jpn. Ser.*
436 *II*, 48(4), 331–347, <https://doi.org/10.2151/jmsj1965.48.4331>, 1970b.

437 Yanai, M., and M. Lu: Equatorially trapped waves at the 200 mb level and their association with meridional convergence of
438 wave energy flux, *J. Atmos. Sci.*, 40, 2785–2803, [https://doi.org/10.1175/1520-0469\(1983\)040<2785>2.0.CO;2](https://doi.org/10.1175/1520-0469(1983)040<2785>2.0.CO;2), 1983.

439 Yang, G., B. Hoskins, and J. Slingo: Convectively coupled equatorial waves: A new methodology for identifying wave
440 structures in observational data, *J. Atmos. Sci.*, 60, 1637–1654, [https://doi.org/10.1175/1520-0469\(2003\)060<1637>2.0.CO;2](https://doi.org/10.1175/1520-0469(2003)060<1637>2.0.CO;2), 2003.

442 Yang, G.-Y., and Hoskins, B. J.: ENSO-related variation of equatorial MRG and Rossby waves and forcing from higher
443 latitudes, *Q. J. R. Meteorol. Soc.*, 142, 2488–2504, <https://doi.org/10.1002/qj.2842>, 2016.

- 444 Yang, G., and Hoskins, B. J.: The equivalent barotropic structure of waves in the tropical atmosphere in the Western
445 Hemisphere, *J. Atmos. Sci.*, 74, 1689–1704, <https://doi.org/10.1175/JAS-D-16-0267.1>, 2017.
- 446 Yang, G., Methven, J., Woolnough, S., Hodges, K., and Hoskins, B.: Linking African easterly wave activity with equatorial
447 waves and the influence of Rossby waves from the Southern Hemisphere, *J. Atmos. Sci.*, 75, 1783–1809,
448 <https://doi.org/10.1175/JAS-D-17-0184.1>, 2018.
- 449 Zhou, X., and B. Wang: Transition from an eastern Pacific upper-level mixed Rossby-gravity wave to a western Pacific
450 tropical cyclone, *Geophys. Res. Lett.*, 34, L24801, <https://doi.org/10.1029/2007GL031831>, 2007.
- 451 Zhang, C., and P. J. Webster: Laterally forced equatorial perturbations in a linear model. Part I: Stationary transient forcing,
452 *J. Atmos. Sci.*, 49, 585–607, [https://doi.org/10.1175/1520-0469\(1992\)049<0585>2.0.CO;2](https://doi.org/10.1175/1520-0469(1992)049<0585>2.0.CO;2), 1992.